



Article

# A ‘Turn-On’ Carbamazepine Sensing Using a Luminescent $\text{SiO}_2$ - $\text{-(CH}_2\text{)}_3\text{NH}_2$ - $\text{-C}_6\text{H}_5$ + Rh6G System

Halyna Yankovych \* , Erika Dutková , Viktoriia Kyshkarova, Miroslava Vaclavikova and Inna Melnyk \*

Institute of Geotechnics, Slovak Academy of Sciences, Watsonova 45, 04001 Kosice, Slovakia

\* Correspondence: yankovych@saske.sk (H.Y.); melnyk@saske.sk (I.M.)

**Abstract:** Carbamazepine is a crucial medication used to treat nervous system disorders, and its low level of absorption in the human body suggests that a significant amount of it may be present in sewage water. Consequently, this pioneering research deals with the synthesis and application of a luminescent sensor based on rhodamine 6 G-modified bifunctional silica particles for the determination of carbamazepine. The sensing material was fabricated in one step by the sol–gel technique and the dye was adsorbed onto the surface from an alcohol solution. The composition, morphology and size of functionalized silica particles were determined by physico-chemical methods. The material’s features provide the possibility of its application as a sensing material for carbamazepine determination at a variety of concentrations. The sensor possesses a linear response towards carbamazepine in the concentration range of 0.8–200.0  $\mu\text{M}$  with a limit of detection (LOD) of 17.9  $\mu\text{M}$  and a limit of quantification (LOQ) of 59.7  $\mu\text{M}$  and has demonstrated reliable quantification over a wide range of concentrations, from therapeutic to high fatal concentrations. Additionally, the sensing mechanism has been proposed, which involves the formation of hydrogen bonding between carbamazepine and Rhodamine 6G immobilized bifunctional silica particles.

**Keywords:** luminescent sensor; drug detection; silica microspheres; Rhodamine 6G; pharmaceutical pollution



**Citation:** Yankovych, H.; Dutková, E.;

Kyshkarova, V.; Vaclavikova, M.;

Melnyk, I. A ‘Turn-On’

Carbamazepine Sensing Using a  
Luminescent  $\text{SiO}_2$ - $\text{-(CH}_2\text{)}_3\text{NH}_2$ /  
 $\text{-C}_6\text{H}_5$  + Rh6G System. *Chemosensors*  
2023, 11, 332. <https://doi.org/10.3390/chemosensors11060332>

Academic Editor: Xin Zhou

Received: 30 March 2023

Revised: 29 May 2023

Accepted: 30 May 2023

Published: 4 June 2023



**Copyright:** © 2023 by the authors. Licensee MDPI, Basel, Switzerland. This article is an open access article distributed under the terms and conditions of the Creative Commons Attribution (CC BY) license (<https://creativecommons.org/licenses/by/4.0/>).

## 1. Introduction

A considerable outtake of drugs released both from domestic and hospital units threatens the environment through undesirable ingestion and production of resistant bacteria, leading to severe impacts on public health. Pharmaceutical pollution possesses additional risks to the environmental microbiome and, moreover, disrupts the gut microbiota in the human body [1]. Therefore, it is important to develop a reliable, sensitive and simple analytical technique for the detection and quantitative determination of drugs and their residues.

Carbamazepine (Figure 1) is an essential medicine utilized for the treatment of seizures, trigeminal neuralgia, behavioral disorders in adults and children [2], schizophrenia, bipolar disorders, and—in combination with other medicaments—is helpful in alcohol withdrawal therapy [3]. It is the only drug that is licensed by the Food and Drug Administration for trigeminal neuralgia therapy [4]. The treatment mechanism consists of blocking sodium channels, which leads to the inhibition of the depolarization rate and reduction of cell excitability [5]. The therapeutic dosage of carbamazepine in plasma is set at the range of 4–12  $\mu\text{g}\cdot\text{L}^{-1}$  [6]. Carbamazepine is metabolized in the liver with the formation of at least 33 known metabolites [3]. However, water quality service has revealed that carbamazepine is one of the most commonly identified drugs in household wastewater and, subsequently, in rivers [7]. According to [8], the concentration range varies from 0.035 to 6.3  $\mu\text{g}\cdot\text{L}^{-1}$ .

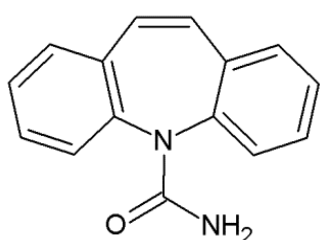


**Figure 1.** Structural formula of carbamazepine (5H-dibenz(b,f)azepine-5-carboxamide).

Among carbamazepine determination methods, several analytical approaches are used: liquid and gas chromatography in combination with mass spectrometry [9,10], immunochromatographic assay [11], electrochemistry [12], sequential injection analysis [13], spectrophotometry [14,15] and luminescence [16,17]. However, most of them require special expensive equipment and highly-skilled operators, which cause additional expenses.

Luminescence is a very good alternative for avoiding these complications, due to its features: high signal intensity, specificity, selectivity and high sensitivity—and is easy to operate. Meanwhile, the luminescent sensors based on nanoparticles are perspective-sensing materials combined with a strong luminescence emission and high quantum yield, longer sensor lifetime, and the possibility of controllable synthesis and functionalization [18]. Since silica nanoparticles do not possess self-luminescent properties, their role as optical sensors is underestimated. This group of nanoparticles has great potential, owing to the flexibility of the synthesis route that allows obtaining particles with the desired size, shape, surface area and controllable surface features [19]. Moreover, the functionalization of silica nanoparticles is simple and effective with the possibility to increase their biocompatibility. The anchoring of a fluorescent dye onto the nanoparticles' surface improves the selectivity and sensitivity of the developed sensor [20]. The combination of features of silica nanoparticles and fluorescent dye enhances the luminescent properties of the dye due to increased quantum yield and reduced quenching, which in turn makes the system useful in pharmaceutical sensing.

Herein, Rhodamine 6G (Rh6G) was utilized to enhance the luminescent properties of bifunctional silica particles with 3-aminopropyl and phenyl groups. Rhodamine 6G is a fluorescent dye, which is commonly employed as a fluorescence reference material owing to exceptional photostability and high quantum yield [21]. Furthermore, this fluorescent dye has been extensively used in the development of sensing probes for the determination of various analytes, such as Fe(III) [22], Cu(II) and Hg(II) [23], Al(III) and Cr(III) [24], cysteine [25], and hyaluronidase [26], due to its exceptional metrological characteristics. The chemical structure of Rh6G enables its modification and attachment to the surface while preserving its fluorophore properties, which is advantageous for achieving high sensor sensitivity and selectivity. Therefore, the development of the sensor was realized by the attachment of Rh6G dye to the bifunctional silica by two approaches: adsorption of the dye on the silica surface and direct incorporation of dye during the synthesis of silica NPs. Three materials were produced— $\text{SiO}_2/\equiv\text{Si}(\text{CH}_2)_3\text{NH}_2/\equiv\text{SiC}_6\text{H}_5$ ,  $\text{SiO}_2/\equiv\text{Si}(\text{CH}_2)_3\text{NH}_2/\equiv\text{SiC}_6\text{H}_5 + \text{Rh6G (ads.)}$  and  $\text{SiO}_2/\equiv\text{Si}(\text{CH}_2)_3\text{NH}_2/\equiv\text{SiC}_6\text{H}_5 + \text{Rh6G (synt.)}$ . The synthesized materials were characterized by SEM, GSA, IR, DLS, TGA, acid-base titration analytical techniques, and  $\zeta$ -potential measurements. The luminescent properties were monitored by photoluminescence spectroscopy. The highest sensor response was obtained for the  $\text{SiO}_2/\equiv\text{Si}(\text{CH}_2)_3\text{NH}_2/\equiv\text{SiC}_6\text{H}_5 + \text{Rh6G (ads.)}$  sample. The main analytical characteristics of the developed sensor were estimated: linearity range, limits of detection (LOD), limits of quantification (LOQ), and selectivity. The influence of pH, suspension concentration and stability, ionic strength, and contact time on the sensor response was evaluated. The assumption related to the sensing mechanism has been made, which determines the novelty of this work. Based on the experimental data, the developed luminescent sensor possesses a satisfactory result in the qualitative and quantitative determination of carbamazepine by a simple, fast and reliable analytical procedure.

## 2. Materials and Methods

### 2.1. Chemicals

All chemicals were at least of analytical grade without additional treatment before usage. Reagents applied for the synthesis of silica microspheres: tetraethyl orthosilicate TEOS ( $\text{Si}(\text{OC}_2\text{H}_5)_4$ , 98%, Alfa Aesar, Kandel, Germany), 3-aminopropyltriethoxysilane APTES ( $\text{NH}_2(\text{CH}_2)_3\text{Si}(\text{OC}_2\text{H}_5)_3$ , 99%, Acros Organics, Geel, Belgium), phenyltriethoxysilane PhTES ( $\text{C}_6\text{H}_5\text{Si}(\text{OC}_2\text{H}_5)_3$ , 98%, Alfa Aesar, Karlsruhe, Germany), ethyl alcohol EtOH ( $\text{C}_2\text{H}_5\text{OH}$ , 96%, mikroCHEM, Pezinok, Slovakia), ammonium solution ( $\text{NH}_3 \cdot \text{H}_2\text{O}$ , 25%, p.a., CentralChem®, Bratislava, Slovakia), and Rhodamine 6G ( $\text{C}_{28}\text{H}_{31}\text{N}_2\text{O}_3\text{Cl}$ , 99%, Acros Organics, Geel, Belgium).

Chemicals used in luminescent tests: carbamazepine ( $\text{C}_{15}\text{H}_{12}\text{N}_2\text{O}$ , 98%, Alfa Aesar, Kandel, Germany), KCl (99.5%, mikroCHEM, Pezinok, Slovakia), NaOH (p.a., CentralChem®, Bratislava, Slovakia), HCl (35%, mikroCHEM, Pezinok, Slovakia), and methyl orange (p.a., Lachema, Brno, Czech Republic). As interferents, ofloxacin ( $\text{C}_{18}\text{H}_{20}\text{FN}_3\text{O}_4$ , 98%, Acros Organics, Geel, Belgium), ciprofloxacin ( $\text{C}_{17}\text{H}_{18}\text{FN}_3\text{O}_3$ , 98%, ThermoScientific, Kandel, Germany), doxycycline monohydrate ( $\text{C}_{22}\text{H}_{24}\text{N}_2\text{O}_8 \cdot \text{H}_2\text{O}$ , 98%, ThermoScientific, Kandel, Germany), flumequine ( $\text{C}_{14}\text{H}_{12}\text{FNO}_3$ , 98%, ThermoScientific, Kandel, Germany), norfloxacin ( $\text{C}_{16}\text{H}_{18}\text{FN}_3\text{O}_3$ , 98%, ThermoScientific, Kandel, Germany), and enrofloxacin ( $\text{C}_{19}\text{H}_{22}\text{FN}_3\text{O}_3$ , 98%, ThermoScientific, Kandel, Germany) were used with a concentration of 200  $\mu\text{M}$  for each drug, as well as urea ( $\text{CH}_4\text{N}_2\text{O}$ , 99.5%, Sklochem-Agroekolab) with concentration 3000  $\mu\text{M}$ , glucose ( $\text{C}_6\text{H}_{12}\text{O}_6 \cdot \text{H}_2\text{O}$ , p.a., ITES Vranov, Presov, Slovakia)—2300  $\mu\text{M}$ , glycine ( $\text{C}_2\text{H}_5\text{O}_2\text{N}$ , p.a., Lachema, Brno, Czech Republic)—7555  $\mu\text{M}$ , phosphate  $\text{PO}_4^{3-}$  (phosphate buffered saline tablets, Fisher Bioreagents, Geel, Belgium)—2500  $\mu\text{M}$ , and  $\text{Ca}^{2+}$  (in form of anhydrous  $\text{CaCl}_2$ , 93%, Sigma)—67.6  $\mu\text{M}$ .

### 2.2. Sol–Gel Synthesis of the Materials

The synthesis of silica-based materials was performed according to [27] with few modifications (see schemes in Figure 2). For this purpose, TEOS (0.0448 mol), APTES (0.0146 mol) and PhTES (0.00745 mol) were mixed with EtOH (100 mL), implying that amino groups from APTES would catalyze the reaction at the early stage. Then, after 1 h  $\text{NH}_4\text{OH}$  (5 mL) was added to finalize the process. After 1 h of stirring, the sample was separated by centrifugation, washed with ethanol and dried in an oven at 80 °C for 24 h. This sample was labeled as  $\text{SiO}_2/\equiv\text{Si}(\text{CH}_2)_3\text{NH}_2/\equiv\text{SiC}_6\text{H}_5$ .

The sample  $\text{SiO}_2/\equiv\text{Si}(\text{CH}_2)_3\text{NH}_2/\equiv\text{SiC}_6\text{H}_5 + \text{Rh6G (ads.)}$  was obtained from 1 g of  $\text{SiO}_2/\equiv\text{Si}(\text{CH}_2)_3\text{NH}_2/\equiv\text{SiC}_6\text{H}_5$  which was mixed with 0.035 g (0.000073 mol) of Rh6G in 100 mL of EtOH at 65 °C for 1 h.

The one-step fixation of the dye onto the surface of the microspheres was carried out as follows: 0.07 g (0.000146 mol) of Rh6G in 50 mL of EtOH was mixed with APTES (0.0146 mol) and PhTES (0.00745 mol). The solution was stirred and heated to 65 °C for 1 h. After cooling, 50 mL of ethyl alcohol, 10 mL (0.0448 mol) of TEOS, and 5 mL of  $\text{NH}_4\text{OH}$  were added. After 1 h of stirring, the sample was separated by centrifugation, washed with ethanol and dried in an oven at 80 °C for 24 h. This sample was labelled  $\text{SiO}_2/\equiv\text{Si}(\text{CH}_2)_3\text{NH}_2/\equiv\text{SiC}_6\text{H}_5 + \text{Rh6G (synt.)}$ . Based on references [28,29], it has been observed that the quantum yield of Rhodamine 6G decreases with an increase in concentration (above  $2 \times 10^{-4}$  M) due to self-quenching. Consequently, it was hypothesized that the optimal proportion of fluorophore and nanoparticles would yield the highest quantum yield, as at this concentration of Rhodamine 6G the formation of dimers and trimers is minimized [28].

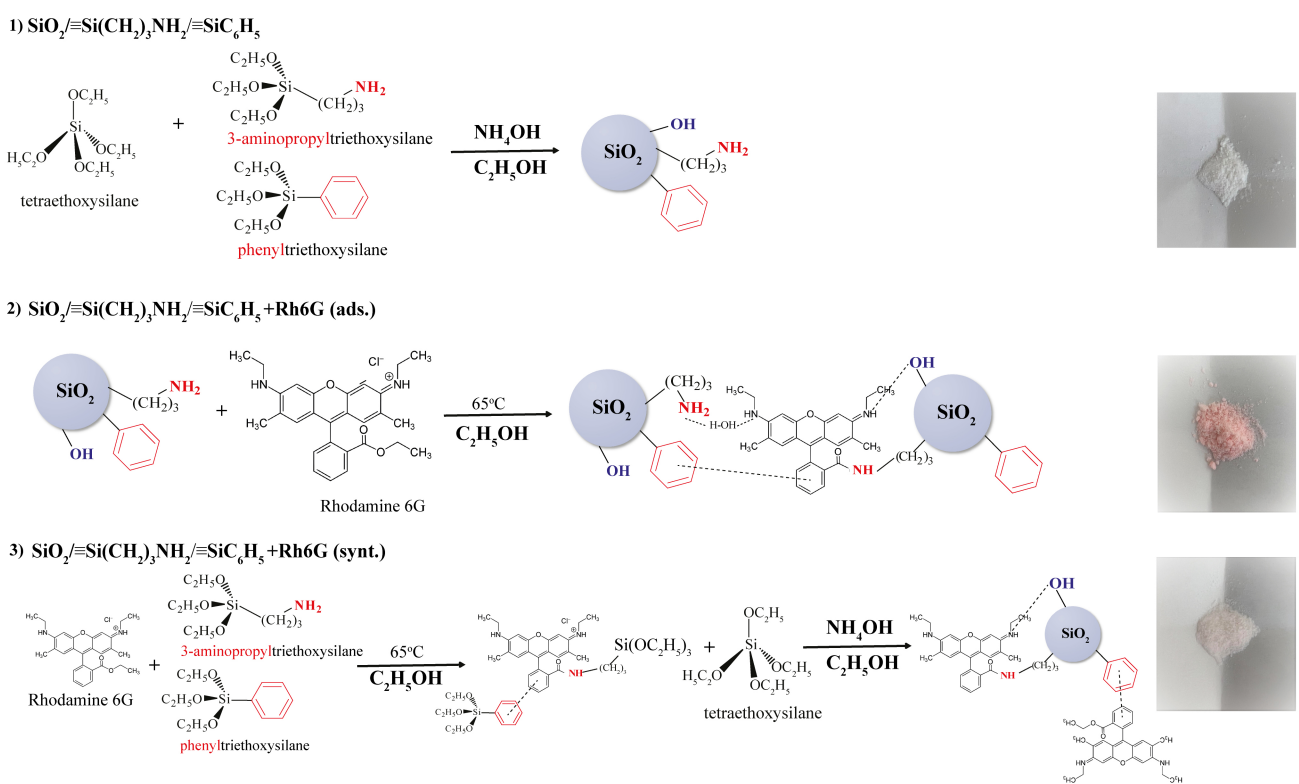


**Figure 2.** Synthesis schemes of bare bifunctional silica particles (1) and functionalized with Rhodamine 6G (2), (3).

### 2.3. Characterization Techniques

The samples' surface morphology was examined by the Zeiss SUPRA 55VP, a scanning electron microscope (SEM) with a field emission electron gun (FEG). In order to avoid the build-up of positive charges and achieve contrasting images, a thin, continuous layer of gold was applied to the surface of the samples using cathodic sputtering in a vacuum.

Fourier Transform Infrared (FTIR) spectra were obtained on FTIR Spectrometer Tensor 27 (Bruker Optik GmbH, Ettlingen, Germany) in the range of 4000–400 cm<sup>-1</sup>, with the resolution step of 2 cm<sup>-1</sup> using KBr pellets. The pellets were heated at 100 °C before recording.

The BET surface area of each sample was estimated from the nitrogen adsorption isotherms at –196 °C, measured by a NOVA 1200e Surface Area & Pore Size Analyzer (Quantachrome Instruments, Boynton Beach, FL, USA). For this purpose, the samples were degassed at 100 °C in a vacuum under pressure below 2 Pa for 24 h. The data from the adsorption part of the isotherm were processed by the BET (Brunauer–Emmett–Teller) equation using the range of relative pressure p/p<sub>0</sub> 0.05–0.35 to calculate a specific surface area. The total pore volume (V<sub>tot</sub>) was obtained from the maximum nitrogen adsorbed volume at relative pressure close to the saturation pressure.

Measurements of  $\zeta$ -potential were carried out on Zetasizer Nano ZS (Malvern, Great Britain). The prepared 1% suspensions in 0.001 M KCl were left for 2 h and then sonicated for 30 min. The pH was adjusted by the addition of 0.1 M NaOH and 0.1 M HCl using the MeterLab PHM210 pH meter.

Particle size distribution was investigated on the same device with 1 mg·mL<sup>-1</sup> sample concentration using ultrapure water (PURELAB® flex) as a solvent.

The acid-base titration of each sample, in order to estimate the amount of available amino surface groups, was conducted using methyl orange as an indicator. The procedure was as follows: 50 mg of the sample was poured with 20 mL of 0.05 M HCl. The suspension was mixed on a magnetic stirrer at 200 rpm for 24 h. Then, the suspension was filtered through Whatman® filter paper and titrated by 0.025 M NaOH in the presence of methyl

orange. The solutions of HCl and NaOH were standardized before the analysis by the same procedure. The number of amino groups per gram of the sample was calculated from the titration data.

The thermogravimetric analysis was performed on the NETZSCH STA 449F3 derivatograph operating in the range of 25–800 °C with a heating rate of 10 °C·min<sup>-1</sup> under a synthetic air atmosphere.

The Vario MACRO cube, an elementary analyzer manufactured by Elementar Analysensysteme GmbH in Germany, was used to analyze the CHN elements in the studied materials.

The concentration of Rh6G in the starting solution and after adsorption was determined by a Helios Gamma UV-Vis spectrophotometer (Thermo electron corporation, Warwickshire, UK) by measuring the dye absorbance at 526.5 nm.

The room temperature photoluminescence (PL) spectra were acquired on a photon-counting spectrofluorometer PC1 (ISS, San Jose, CA, USA) with a photoexcitation wavelength of 480 nm (resolution step 2 nm). A 300 W xenon lamp was used as the excitation source. Excitation and emission slit widths were set at 1.0 and 0.5 mm. The samples were placed into 1 cm path-length rectangular quartz cuvettes for spectral analysis.

#### 2.4. Photoluminescent Method of Carbamazepine Determination

The stock suspensions of  $\text{SiO}_2/\equiv\text{Si}(\text{CH}_2)_3\text{NH}_2/\equiv\text{SiC}_6\text{H}_5$ ,  $\text{SiO}_2/\equiv\text{Si}(\text{CH}_2)_3\text{NH}_2/\equiv\text{SiC}_6\text{H}_5 + \text{Rh6G}$  (ads.) and  $\text{SiO}_2/\equiv\text{Si}(\text{CH}_2)_3\text{NH}_2/\equiv\text{SiC}_6\text{H}_5 + \text{Rh6G}$  (synt.) (0.2 g·L<sup>-1</sup>) used in the analysis were obtained by dissolving an appropriate amount of each sample in 25 mL of solvent and then sonicating for 1 h to destroy particle agglomerates and obtain uniform particle distribution in the bulk of the solvent. A definite concentration of suspension was prepared immediately before the analysis by diluting the stock solution. The analysis of carbamazepine was carried out by the following procedure: An amount of 1.5 mL of stock suspension was mixed with a different amount of carbamazepine stock solution with a concentration of 400 μM and diluted to 3 mL with 0.1 M KCl. Then, the obtained solutions were thoroughly mixed and the photoluminescence spectra in the range of 500–650 nm and excitation wavelength of 480 nm were recorded. The linearity of sensor response was evaluated in the carbamazepine concentration range of 0.8–200 μM. The limit of detection (LOD) and limit of quantification (LOQ) were calculated from data obtained from the calibration curve (CC) for carbamazepine using  $3\sigma/s$  and  $10\sigma/s$  criteria, respectively [30]. Additionally, the sensor response towards carbamazepine was tested in the presence of ofloxacin, ciprofloxacin, doxycycline, flumequine, norfloxacin, enrofloxacin at a concentration of 200 μM for each drug, as well as urea with a concentration of 3000 μM, glucose—2300 μM, glycine—7555 μM, phosphate anions  $\text{PO}_4^{3-}$ —2500 μM, and calcium cations  $\text{Ca}^{2+}$ —67.6 μM [31]. Urea, glucose, glycine, phosphate and calcium were chosen as interferents because of their availability in human serum and urine components [32]. All measurements were performed three times and the error of photoluminescence measurements was 2%.

### 3. Results

It is known from our previous work [33] that silica microspheres can adsorb dyes of various natures and that the presence of hydrophobic adsorption centers increases the value of sorption capacity. It was also shown that the presence of hydrophobic groups on the surface contributes to the preservation of the fluorescent properties of the dye on the carrier. Therefore, silica microspheres with amino and phenyl groups were chosen as a substrate. In addition, the sample  $\text{SiO}_2/\equiv\text{Si}(\text{CH}_2)_3\text{NH}_2/\equiv\text{SiC}_6\text{H}_5 + \text{Rh6G}$  (synt.) was expected to have a chemically fixed dye due to the interaction of the amino group on the surface and ethoxycarbonyl group of the dye [34] (Figure 2).

#### 3.1. Physico-Chemical Properties of Synthesized Materials

In order to estimate the morphology of the samples before and after functionalization with Rh6G, SEM images were obtained. As is evidenced from Figure 3a,c,e, the particle size

is up to 100 nm; it is smaller in the synthesized sample, but they are not individual and form agglomerates. In addition, the smaller particles have distinct spherical contours, which agglomerate in suspension with sizes up to 280 nm (Figure 3b,d,f). The tendency to decrease particle size in line  $\text{SiO}_2/\equiv\text{Si}(\text{CH}_2)_3\text{NH}_2/\equiv\text{SiC}_6\text{H}_5 \geq \text{SiO}_2/\equiv\text{Si}(\text{CH}_2)_3\text{NH}_2/\equiv\text{SiC}_6\text{H}_5 + \text{Rh6G (ads.)} > \text{SiO}_2/\equiv\text{Si}(\text{CH}_2)_3\text{NH}_2/\equiv\text{SiC}_6\text{H}_5 + \text{Rh6G (synt.)}$  can be probably explained by deceleration of the hydrolysis step of the total synthesis process by the presence of Rhodamine 6G, which can act as an electrophile in the system. The values of the average diameter of the particles in the aqueous solution decrease, apparently due to the fact that the charge on the surface increases and the particles stick together less (Figure 3b,d,f). In addition, the SEM image for the sample  $\text{SiO}_2/\equiv\text{Si}(\text{CH}_2)_3\text{NH}_2/\equiv\text{SiC}_6\text{H}_5 + \text{Rh6G (ads.)}$  differs from the others due to the appearance of strong photoluminescence spots.

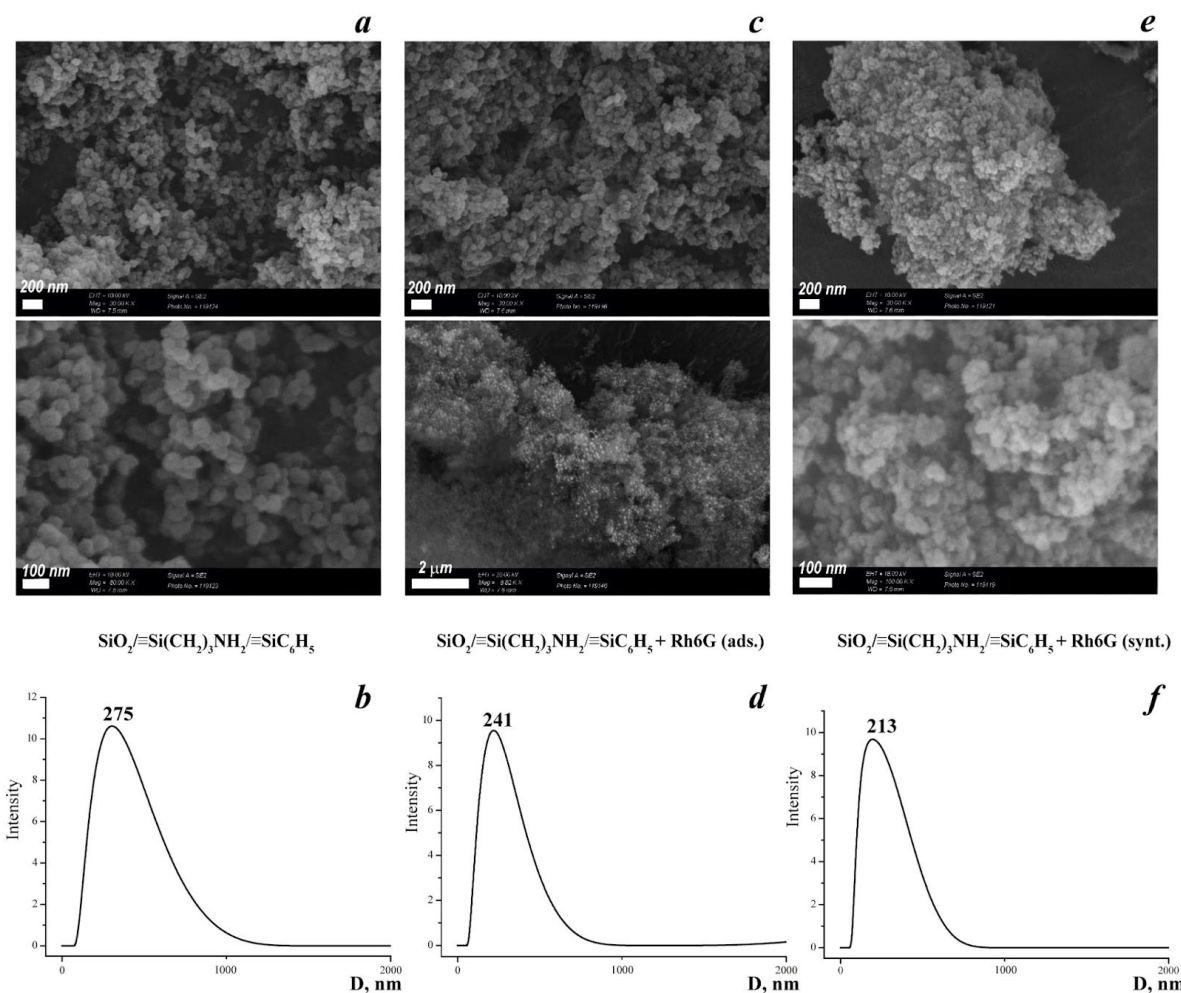


**Figure 3.** SEM images of the synthesized materials (a,c,e) with the corresponding particle size distribution (b,d,f) obtained from DLS data.

The textural properties of synthesized materials were examined by gas sorption analysis. Nitrogen adsorption–desorption isotherms are represented in Figure 4. The shapes of the isotherms revealed the non-porous nature of the  $\text{SiO}_2/\equiv\text{Si}(\text{CH}_2)_3\text{NH}_2/\equiv\text{SiC}_6\text{H}_5$  and  $\text{SiO}_2/\equiv\text{Si}(\text{CH}_2)_3\text{NH}_2/\equiv\text{SiC}_6\text{H}_5 + \text{Rh6G (ads.)}$  samples. According to IUPAC classification [35], the isotherms are related to Type II isotherms. This means that the surface area of synthesized materials is created by particle packing. A small sharp hysteresis loop describes the slit-shaped interparticle pores. The calculated values of  $S_{\text{BET}}$  of the materials are  $149 \text{ m}^2 \cdot \text{g}^{-1}$  for  $\text{SiO}_2/\equiv\text{Si}(\text{CH}_2)_3\text{NH}_2/\equiv\text{SiC}_6\text{H}_5$ , with a total pore volume of  $1.088 \text{ cm}^3 \cdot \text{g}^{-1}$  and  $72 \text{ m}^2 \cdot \text{g}^{-1}$  for  $\text{SiO}_2/\equiv\text{Si}(\text{CH}_2)_3\text{NH}_2/\equiv\text{SiC}_6\text{H}_5 + \text{Rh6G (ads.)}$ , with a total pore volume of  $0.565 \text{ cm}^3 \cdot \text{g}^{-1}$ . Such changes indicate the filling of the space between

the particles, that is, the presence of a dye on the surface of the silica particles. However, the sample  $\text{SiO}_2/\equiv\text{Si}(\text{CH}_2)_3\text{NH}_2/\equiv\text{SiC}_6\text{H}_5 + \text{Rh6G}$  (synt.) possesses higher values of active surface area and total pore volume— $407 \text{ m}^2\cdot\text{g}^{-1}$  and  $1.275 \text{ cm}^3\cdot\text{g}^{-1}$ , respectively, regardless of the Rh6G dye presence and the small difference in particle size (Figure 3). Such changes in textural properties can be interpreted by steric hindrances in material ordering during the synthesis in the presence of a large dye molecule. That is, the dye acted as a kind of ‘template’ during the synthesis, and the part of it that did not bond to the surface of the particles was washed out during washing.

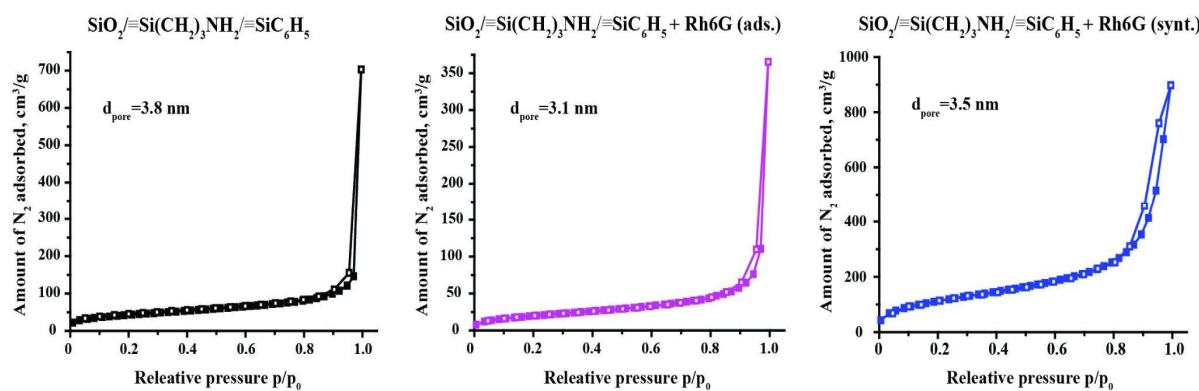


**Figure 4.**  $\text{N}_2$  adsorption-desorption isotherms of studied materials.

Zeta potential is a measure of the electrical potential difference between a particle or a surface and the surrounding fluid. It is an important parameter in the study of colloidal systems, where particles are suspended in a liquid medium. Zeta potential and surface charge are both related to the electrical properties of surfaces and interfaces. Thus, the zeta potential of suspensions at an ionic strength of 1 mM was measured (Figure 5). Therefore, at the natural (~8) pH of the suspensions, the values of the zeta-potential are positive, which indicates the protonation of accessible nitrogen-containing groups on the surface of the samples. Based on these data, samples that contain Rh6G dye exhibit higher zeta-potential values. This is likely due to the presence of two additional nitrogen atoms in the dye. Their availability and possible ‘mobility’ are also important. In the case of physical adsorption for the  $\text{SiO}_2/\equiv\text{Si}(\text{CH}_2)_3\text{NH}_2/\equiv\text{SiC}_6\text{H}_5 + \text{Rh6G}$  (ads.) sample, this behavior of the dye on the surface is reflected in the values of the zeta-potential of the suspension, while attachment of the Rh6G in the case of  $\text{SiO}_2/\equiv\text{Si}(\text{CH}_2)_3\text{NH}_2/\equiv\text{SiC}_6\text{H}_5 + \text{Rh6G}$  (synt.) fixes the dye, and it is also possible that the dye shields the amino groups of the surface.

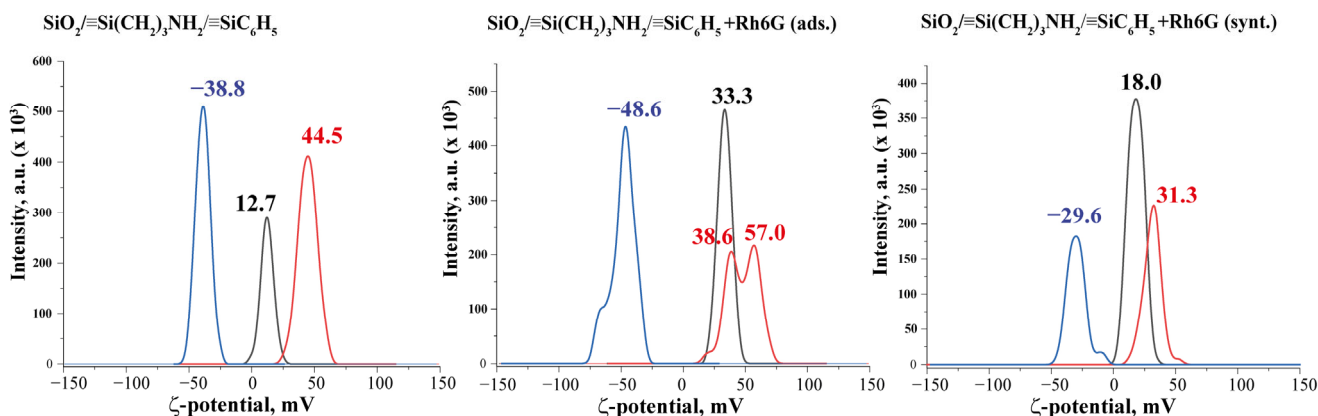


**Figure 5.** Changes in the z-potential values of sample suspensions at different pH: pH = 11—blue curves, pH~8 (initial suspensions)—black curves, and pH = 2—red curves (background 1 mM KCl).

Since the influence of pH on the intensity of photoluminescence of suspensions was studied (see below), changes in the electrokinetic potential of suspensions at different pH levels were investigated (Figure 5). Thus, sample  $\text{SiO}_2/\equiv\text{Si}(\text{CH}_2)_3\text{NH}_2/\equiv\text{SiC}_6\text{H}_5$  has naturally changed the surface charge depending on the pH, to a positive charge in acidic pH and to a negative charge in alkaline pH. The changes in values were greater when adding  $\text{OH}^-$ , as this sample has acceptors for protons. Interesting observations were made for sample  $\text{SiO}_2/\equiv\text{Si}(\text{CH}_2)_3\text{NH}_2/\equiv\text{SiC}_6\text{H}_5 + \text{Rh6G (ads.)}$ , the range of zeta-potential change at pH = 10 was even higher than for the initial sample, but in an acidic medium it appeared that some of the groups were not protonated, the surface was heterogeneous. The overlap of the peaks of sample  $\text{SiO}_2/\equiv\text{Si}(\text{CH}_2)_3\text{NH}_2/\equiv\text{SiC}_6\text{H}_5 + \text{Rh6G (synt.)}$  in water and in an acidic medium also indicates less protonation of the sample surface by acid under these conditions but the charge on the surface is distributed evenly.

Using elemental analysis and acid-base titration, the number of nitrogen-containing groups was determined. The following elemental analysis data were obtained:  $\text{SiO}_2/\equiv\text{Si}(\text{CH}_2)_3\text{NH}_2/\equiv\text{SiC}_6\text{H}_5$  (C-12.97%, N-3.09%, H-3.94%),  $\text{SiO}_2/\equiv\text{Si}(\text{CH}_2)_3\text{NH}_2/\equiv\text{SiC}_6\text{H}_5 + \text{Rh6G (ads.)}$  (C-14.02%, N-3.31%, H-3.92%),  $\text{SiO}_2/\equiv\text{Si}(\text{CH}_2)_3\text{NH}_2/\equiv\text{SiC}_6\text{H}_5 + \text{Rh6G (synt.)}$  (C-22.34%, N-4.42%, H-4.79%). Based on these data, it can be concluded that the original sample contains  $2.2 \text{ mmol}\cdot\text{g}^{-1}$  of amino groups. The analysis has shown almost no changes for the sample with adsorbed Rhodamine 6G, but in the sample where the dye was incorporated during synthesis, the number of nitrogen-bearing groups is  $3.2 \text{ mmol}\cdot\text{g}^{-1}$ . These findings are in complete correlation with the titration data.

It was unexpected that the elemental analysis data of the sample with the adsorbed dye differ little from the original sample, although Figure 1 shows that the sample acquires a pink color. The adsorption study showed that under these conditions  $5 \text{ mg}\cdot\text{g}^{-1}$  of Rhodamine 6G is adsorbed, which does not affect the data of the analysis, for which a dose of 20 mg is used. In the case of the synthesized sample, it is difficult to understand from the data of the elemental analysis how much dye has been fixed, because both the dye and the surface of the particles contain carbon and nitrogen atoms.

To confirm the successful anchoring of Rhodamine 6G on a bifunctional silica support, IR spectra were recorded (Figure 6a–c). The interpretation of obtained data revealed the presence of the most intensive absorption bands of  $\nu_{\text{as}}$  ( $\text{Si}-\text{O}-\text{Si}$ ) at  $1000\text{--}1200 \text{ cm}^{-1}$ , which evidenced the formation of a polysiloxane framework. The availability of amino groups was confirmed by  $\delta(\text{NH}_2)$  and  $\nu_{\text{as,sym}}(\text{NH})$  at  $1596 \text{ cm}^{-1}$ ,  $3365 \text{ cm}^{-1}$  and  $3295 \text{ cm}^{-1}$ , respectively. The low-intensity peaks at  $3073 \text{ cm}^{-1}$  and  $3051 \text{ cm}^{-1}$  were assigned to  $\nu(\text{CH})$  of phenyl aromatic rings. On the spectrum related to  $\text{SiO}_2/\equiv\text{Si}(\text{CH}_2)_3\text{NH}_2/\equiv\text{SiC}_6\text{H}_5 + \text{Rh6G (ads.)}$ , the peaks describing the vibrations of free -OH groups had lower intensities than in bare bifunctional silica samples and the additional peaks at  $1844 \text{ cm}^{-1}$  and  $1435 \text{ cm}^{-1}$  were observed. These peaks can be ascribed to the presence of the Rh6G molecules connected to the material's surface. It is interesting to note, that the sample  $\text{SiO}_2/\equiv\text{Si}(\text{CH}_2)_3\text{NH}_2/\equiv\text{SiC}_6\text{H}_5 + \text{Rh6G (synt.)}$  possessed distinct vibrations of xanthene ring in a range of  $1530\text{--}1500 \text{ cm}^{-1}$  and a sharp middle-intensity peak at  $741 \text{ cm}^{-1}$  associated to xanthene ring deformations [36], which are absent on the infrared spectrum of  $\text{SiO}_2/\equiv\text{Si}(\text{CH}_2)_3\text{NH}_2/\equiv\text{SiC}_6\text{H}_5 + \text{Rh6G (ads.)}$ . Moreover, the enhancement of  $\nu_{\text{as,sym}}(\text{NH})$  peak intensities verifies the presence of dye molecules in the sample, since the IR spectrum of Rh6G also contains these vibrations, hence, an additive effect was achieved. The absence of the bands corresponding to free -OH groups at  $3857 \text{ cm}^{-1}$  and  $3740 \text{ cm}^{-1}$  was observed, probably, due to the occurrence of electrostatic interactions between negatively charged hydroxyl groups and positively charged dye molecules.

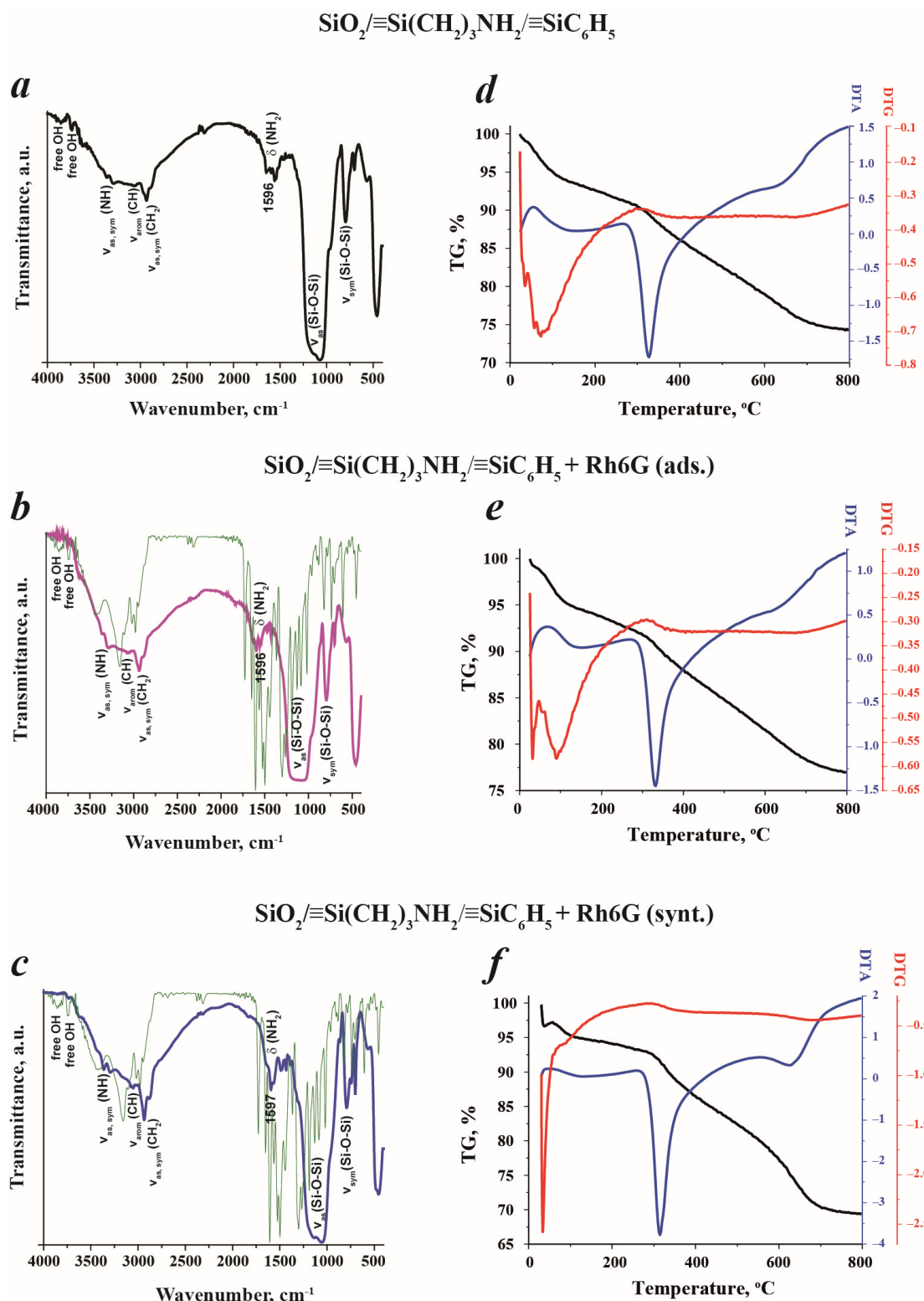


**Figure 6.** Infrared spectra (**a–c**) (green lines—spectra of Rh6G) and corresponding thermograms (**d–f**) of  $\text{SiO}_2/\equiv\text{Si}(\text{CH}_2)_3\text{NH}_2/\equiv\text{SiC}_6\text{H}_5$ ,  $\text{SiO}_2/\equiv\text{Si}(\text{CH}_2)_3\text{NH}_2/\equiv\text{SiC}_6\text{H}_5$  (ads.) and  $\text{SiO}_2/\equiv\text{Si}(\text{CH}_2)_3\text{NH}_2/\equiv\text{SiC}_6\text{H}_5$  (synt.) samples.

Additional investigations of the thermal properties of the synthesized materials were performed. It would seem, at first glance, from the corresponding thermograms in Figure 6d–f, that the thermal behavior of the samples is similar. However, the detailed anal-

ysis highlighted several differences. All samples possessed an exothermic peak in the temperature range of 30–100 °C, which can be assigned to ethanol and water evaporation. The calculated mass losses were as follows: ~2% for  $\text{SiO}_2/\equiv\text{Si}(\text{CH}_2)_3\text{NH}_2/\equiv\text{SiC}_6\text{H}_5$ , ~2.5% for  $\text{SiO}_2/\equiv\text{Si}(\text{CH}_2)_3\text{NH}_2/\equiv\text{SiC}_6\text{H}_5 + \text{Rh6G}$  (ads.), and ~3% for  $\text{SiO}_2/\equiv\text{Si}(\text{CH}_2)_3\text{NH}_2/\equiv\text{SiC}_6\text{H}_5 + \text{Rh6G}$  (synt.). Then, strong endothermic peaks between 100 and 450 °C were observed. These peaks described the oxidation of surface organics of the samples, mainly sensitive to the thermal treatment amino and silanol groups. Nevertheless, the amounts of lost samples' weights were different: 8%, 6.5% and 4.5% for  $\text{SiO}_2/\equiv\text{Si}(\text{CH}_2)_3\text{NH}_2/\equiv\text{SiC}_6\text{H}_5$ ,  $\text{SiO}_2/\equiv\text{Si}(\text{CH}_2)_3\text{NH}_2/\equiv\text{SiC}_6\text{H}_5 + \text{Rh6G}$  (ads.) and  $\text{SiO}_2/\equiv\text{Si}(\text{CH}_2)_3\text{NH}_2/\equiv\text{SiC}_6\text{H}_5 + \text{Rh6G}$  (synt.), respectively. This fact evidenced the formation of new, stronger chemical bonds on the  $\text{SiO}_2/\equiv\text{Si}(\text{CH}_2)_3\text{NH}_2/\equiv\text{SiC}_6\text{H}_5 + \text{Rh6G}$  (ads.) and  $\text{SiO}_2/\equiv\text{Si}(\text{CH}_2)_3\text{NH}_2/\equiv\text{SiC}_6\text{H}_5 + \text{Rh6G}$  (synt.) samples' surfaces that cannot be easily decomposed.

The different values of weight losses demonstrated the different amounts of anchored Rh6G in the samples prepared by different approaches. Indeed, the sample  $\text{SiO}_2/\equiv\text{Si}(\text{CH}_2)_3\text{NH}_2/\equiv\text{SiC}_6\text{H}_5 + \text{Rh6G}$  (synt.) had a lower mass loss in this range and, therefore, a higher amount of bounded Rhodamine 6G, which 'protect' the surface groups from oxidation. It is noteworthy that the low-intensity endothermal peaks in the range of 450–800 °C were recorded and related to the decomposition of organic matter present in the samples, including thermally stable phenyl moieties. The most distinct peak was noticed on the  $\text{SiO}_2/\equiv\text{Si}(\text{CH}_2)_3\text{NH}_2/\equiv\text{SiC}_6\text{H}_5 + \text{Rh6G}$  (synt.) sample's thermogram, with a mass loss of 17.5%. For the bare bifunctional silica sample, this value was 24% and for  $\text{SiO}_2/\equiv\text{Si}(\text{CH}_2)_3\text{NH}_2/\equiv\text{SiC}_6\text{H}_5 + \text{Rh6G}$  (ads.) it was 13%. The total weight loss during the thermal treatment was as follows:  $\text{SiO}_2/\equiv\text{Si}(\text{CH}_2)_3\text{NH}_2/\equiv\text{SiC}_6\text{H}_5$ —36%,  $\text{SiO}_2/\equiv\text{Si}(\text{CH}_2)_3\text{NH}_2/\equiv\text{SiC}_6\text{H}_5 + \text{Rh6G}$  (ads.)—34% and  $\text{SiO}_2/\equiv\text{Si}(\text{CH}_2)_3\text{NH}_2/\equiv\text{SiC}_6\text{H}_5 + \text{Rh6G}$  (synt.)—30%. To summarize the obtained results, the presence of Rhodamine 6G changes the thermal behavior of the fabricated samples due to the functionalization of available groups and improving the stability of free surface moieties.

### 3.2. Investigation of PL Properties of Sensor and Detection Conditions

To determine the photoluminescent properties of the materials synthesized, the photoluminescence spectra of their water suspensions were recorded (Figure 7). As can be seen in Figure 7a, the samples  $\text{SiO}_2/\equiv\text{Si}(\text{CH}_2)_3\text{NH}_2/\equiv\text{SiC}_6\text{H}_5$  and  $\text{SiO}_2/\equiv\text{Si}(\text{CH}_2)_3\text{NH}_2/\equiv\text{SiC}_6\text{H}_5 + \text{Rh6G}$  (synt.) possessed low PL intensity, while  $\text{SiO}_2/\equiv\text{Si}(\text{CH}_2)_3\text{NH}_2/\equiv\text{SiC}_6\text{H}_5 + \text{Rh6G}$  (ads.) showed a satisfied PL response. In order to improve the PL intensity, the samples' suspensions were prepared using 0.1 M KCl to create the ionic strength. Indeed, the increase of PL intensity of  $\text{SiO}_2/\equiv\text{Si}(\text{CH}_2)_3\text{NH}_2/\equiv\text{SiC}_6\text{H}_5 + \text{Rh6G}$  (ads.) was observed (Figure 7b), which can be explained by a greater orderliness of the particles in suspension and, therefore, higher excitation efficiency. Since only this sample showed good PL properties, all subsequent studies were conducted only with this sample.

It is known that several determinative factors have a great influence on luminescence intensity. In this research, the influence of ionic strength, particle concentration, pH and contact time on sensor response was investigated. Figure 8a illustrates the changes in PL intensity of  $\text{SiO}_2/\equiv\text{Si}(\text{CH}_2)_3\text{NH}_2/\equiv\text{SiC}_6\text{H}_5 + \text{Rh6G}$  (ads.) suspensions depending on the suspension concentration and ionic strength. As is evidenced, the increase in concentration leads to an increase in PL intensity, however, the shift in emission maximum and peak deformation were registered. These changes can probably be explained by particle agglomeration. The higher suspension concentrations were not considered due to the possible occurrence of hindrances in the light transmission through highly concentrated suspensions and particle aggregation. Additionally, the ionic strength in the range of 0.05–1.0 M KCl (Figure 8a) had no significant influence on PL response, therefore, the middle KCl concentration was chosen for further studies. The absence of ionic strength caused the decrease in PL intensity as has been shown in Figure 7b. Under these conditions, i.e.,  $0.1 \text{ g}\cdot\text{L}^{-1}$  in 0.1 M KCl, the stability of suspension was examined. The prepared

suspension was stable for up to 5 days with retention of photoluminescent properties (Figure 8b).

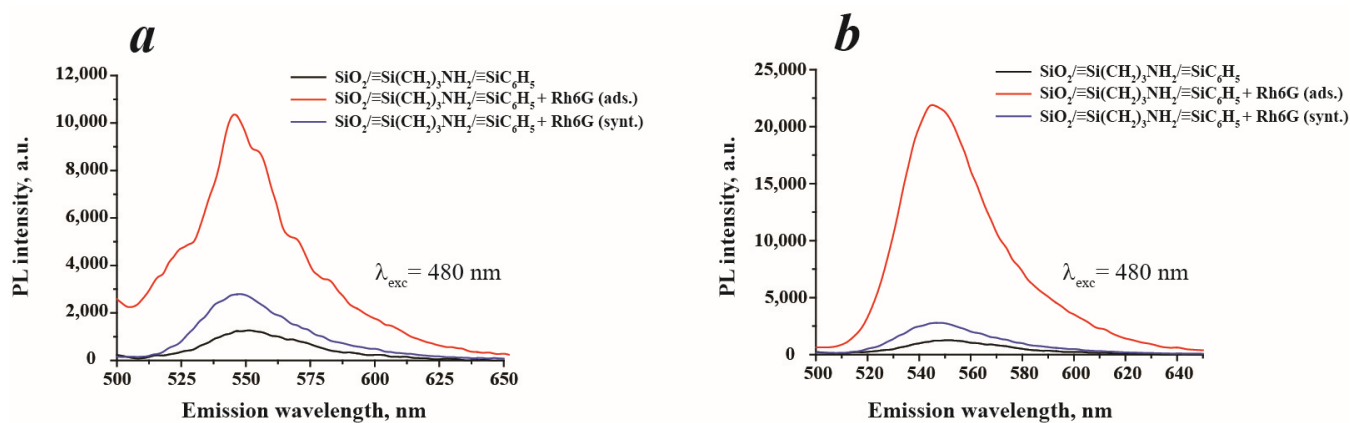


**Figure 7.** Photoluminescence spectra of synthesized materials with a concentration of  $0.1 \text{ g}\cdot\text{L}^{-1}$ : (a)—water and (b)— $0.1 \text{ M KCl}$ .

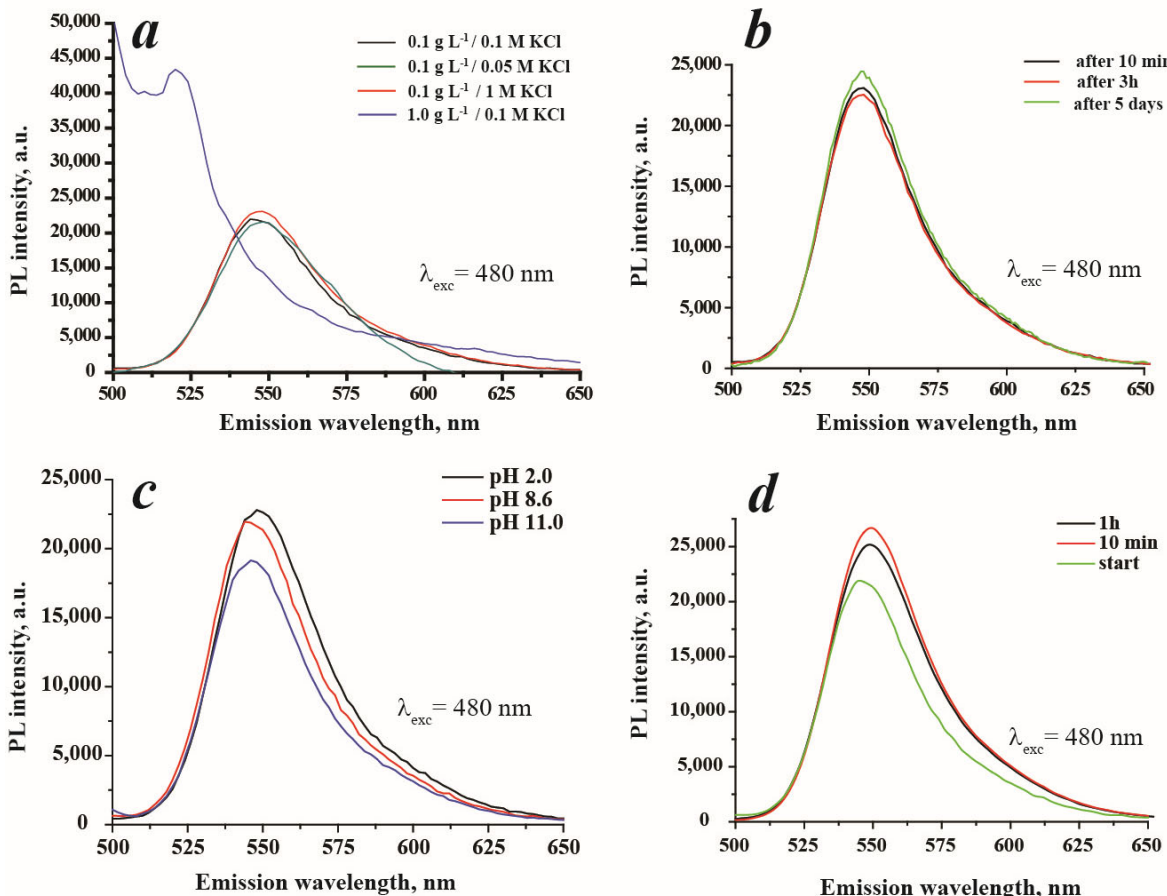


**Figure 8.** Influence of different factors on photoluminescent properties of  $\text{SiO}_2/\equiv\text{Si}(\text{CH}_2)_3\text{NH}_2/\equiv\text{SiC}_6\text{H}_5 + \text{Rh6G}$  (ads.): (a)—influence of suspension concentration and ionic strength on PL intensity, (b)—investigation of suspension stability ( $0.1 \text{ g}\cdot\text{L}^{-1}$  in  $0.1 \text{ M KCl}$ ), (c)—influence of pH on PL intensity (suspension concentration  $0.1 \text{ g}\cdot\text{L}^{-1}$ ), and (d)—kinetics of sensor response in the presence of carbamazepine at  $C = 200 \mu\text{M}$  and  $0.1 \text{ g}\cdot\text{L}^{-1}$  in  $0.1 \text{ M KCl}$  suspension concentration.

It is acknowledged that the photoluminescent properties depend on the pH. Thus, the impact of the pH on the PL intensity of  $\text{SiO}_2/\equiv\text{Si}(\text{CH}_2)_3\text{NH}_2/\equiv\text{SiC}_6\text{H}_5 + \text{Rh6G}$  (ads.) was studied. As is demonstrated in Figure 8c, pH affects the PL intensity, and the increase in pH leads to a decrease in luminescence intensity. Apparently, the quenching is caused by the presence of hydroxyl anions that surround material particles and interact with positively charged dye molecules and amino surface groups. This effect can be described as an intramolecular charge transfer process. The PL intensity of  $\text{SiO}_2/\equiv\text{Si}(\text{CH}_2)_3\text{NH}_2/\equiv\text{SiC}_6\text{H}_5 + \text{Rh6G}$  (ads.) at pH 2 and 8.6 (this pH corresponds to the actual pH of the working suspension) have very close values. This can be interpreted by the similarity of particles' charges (see Figure 4) and, therefore, of their organization in solution. Figure 8d illustrates the influence of contact time between analyte and sensor-on-sensor response. The best sensor response was obtained in the 5–15 min (not detailed) interval, with the small PL quenching at 1 h. The increase of PL at the selected time interval can be probably explained by the arrangement of dye molecules on the surface of the material [29]. The slight decrease of sensor PL after 1 h of incubation can be associated with particle aging and agglomeration. Based on these data, all further analysis was carried out after 10 min from the addition of carbamazepine to the suspension.

The influence of carbamazepine concentration on the luminescence response of a sensor is demonstrated in Figure 9a. As can be seen, the sensor possesses a linear response towards carbamazepine in the concentration range of 0.8–200.0  $\mu\text{M}$  with a correlation coefficient  $R^2 = 0.992$ . The higher concentrations were not considered due to the low solubility of carbamazepine— $<200 \text{ mg}\cdot\text{L}^{-1}$  or 846.4  $\mu\text{M}$  [37]. The limit of detection, LOD, of the sensor was estimated to be 17.9  $\mu\text{M}$  ( $4.2 \text{ mg}\cdot\text{L}^{-1}$ ) and the limit of quantification, LOQ, was 59.7  $\mu\text{M}$  ( $14.1 \text{ mg}\cdot\text{L}^{-1}$ ). In order to evaluate the interfering effect of several antibiotics and smaller organic compounds on sensor response, the selectivity test was performed (Figure 9b). The results revealed the intensive response of the studied system towards flumequine and norfloxacin, which is equivalent to carbamazepine. Therefore, these two compounds have a very strong interfering effect and should be eliminated from the sample before analysis. It has been estimated that the presence of carbamazepine causes the small red shift  $\Delta = 4 \text{ nm}$  of the peak position on the PL spectrum of  $\text{SiO}_2/\equiv\text{Si}(\text{CH}_2)_3\text{NH}_2/\equiv\text{SiC}_6\text{H}_5 + \text{Rh6G}$  (ads.). However, Figure 9c illustrates that the presence of flumequine or norfloxacin does not cause a shift in the sensor's maximum wavelength. This observation can be utilized in the analysis of water samples to selectively determine the presence of carbamazepine. Analytical research data suggest that flumequine and norfloxacin are typically found in water samples within the  $\text{ng}\cdot\text{L}^{-1}$  to low  $\text{mg}\cdot\text{L}^{-1}$  concentration range [38]. Flumequine is rarely detected in water samples due to its tendency to remain in sediments [39], but it can still be detected in water samples at levels up to  $32 \text{ ng}\cdot\text{L}^{-1}$  [40,41]. On the other hand, the concentration of norfloxacin can be higher, ranging from  $489 \text{ ng}\cdot\text{L}^{-1}$  [42] to  $0.12 \text{ mg}\cdot\text{L}^{-1}$  [43]. In the case of ciprofloxacin, doxycycline and enrofloxacin, the PL intensities of  $\text{SiO}_2/\equiv\text{Si}(\text{CH}_2)_3\text{NH}_2/\equiv\text{SiC}_6\text{H}_5 + \text{Rh6G}$  (ads.) were slightly enhanced, which can lead to overestimated results during carbamazepine determination in simultaneous presence in the matrix. Only in the presence of ofloxacin did the sensor show a selective response to carbamazepine. The influence of smaller organic molecules that can be found in human samples, such as urea, glucose, glycine and two inorganic species—phosphate anions and  $\text{Ca}^{2+}$ —was also tested. The highest interfering effect on sensor response was caused by urea, which manifested as a decrease in the PL signal. In the simultaneous presence of carbamazepine and urea in the samples, the underestimated results will be obtained. Other compounds demonstrated a moderate effect on the sensor signal. To summarize, the sensor selectivity can be improved by sample pre-treatment to avoid the interfering impact on the analytical signal.

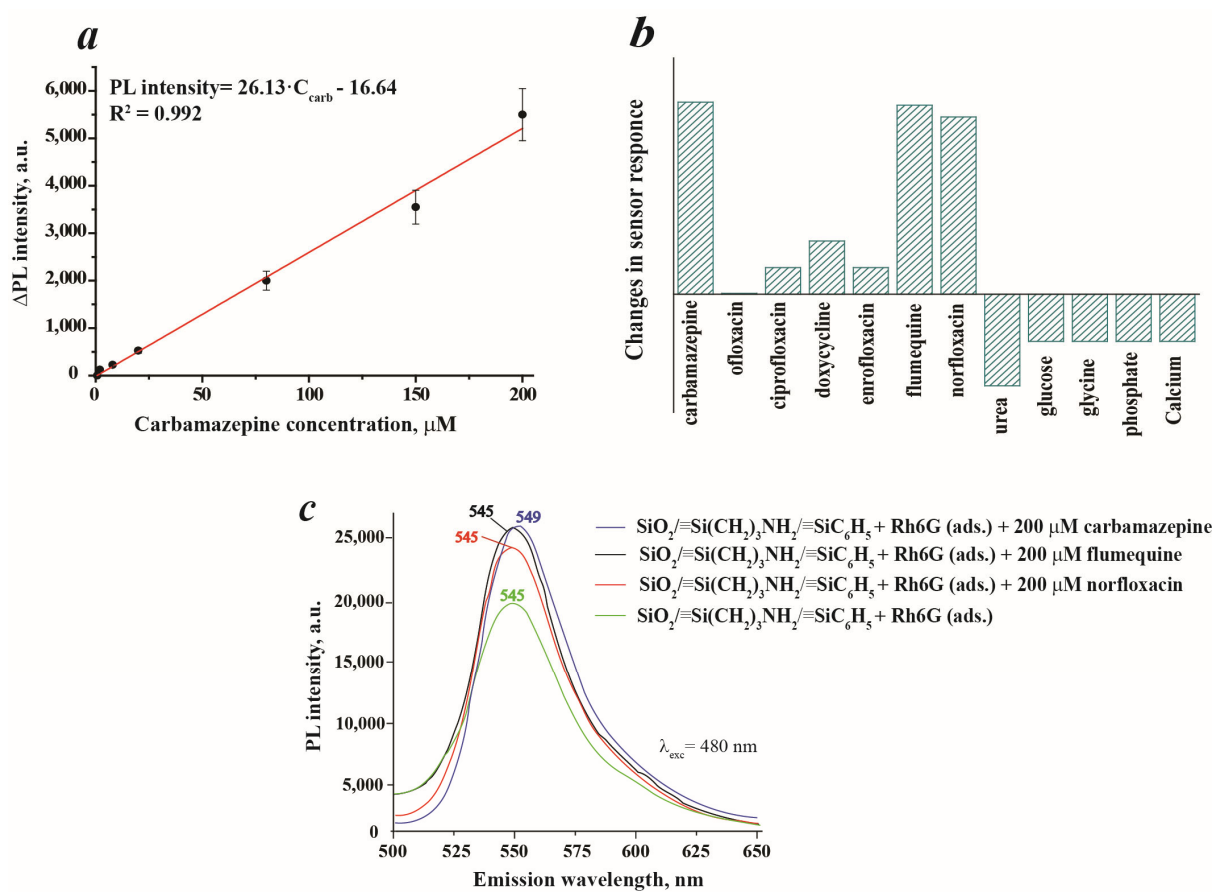


**Figure 9.** Calibration curve of carbamazepine in the concentration range of 0.8–200.0  $\mu\text{M}$  (suspension concentration 0.1 g·L<sup>-1</sup> in 0.1 M KCl): (a); interfering effect of several selected compounds on  $\text{SiO}_2/\equiv\text{Si}(\text{CH}_2)_3\text{NH}_2/\equiv\text{SiC}_6\text{H}_5 + \text{Rh6G (ads.)}$  sensor response (concentration of antibiotics was 200  $\mu\text{M}$ ; urea—3000  $\mu\text{M}$ , glucose—2300  $\mu\text{M}$ , glycine—7555  $\mu\text{M}$ , phosphate anions  $\text{PO}_4^{3-}$ —2500  $\mu\text{M}$  and  $\text{Ca}^{2+}$  cations—67.6  $\mu\text{M}$ ) (b); PL spectra of  $\text{SiO}_2/\equiv\text{Si}(\text{CH}_2)_3\text{NH}_2/\equiv\text{SiC}_6\text{H}_5 + \text{Rh6G (ads.)}$  in the presence of carbamazepine, flumequine and norfloxacin with concentration 200  $\mu\text{M}$  (c).

### 3.3. Possible Physico-Chemical Mechanism of Carbamazepine Sensing

The investigation of the sensing mechanism is an important issue in order to understand the nature of processes occurring during the sensing of the analyte. For this purpose, the blank experiment with Rhodamine 6G has been performed. It has been estimated that the amount of Rh6G in  $\text{SiO}_2/\equiv\text{Si}(\text{CH}_2)_3\text{NH}_2/\equiv\text{SiC}_6\text{H}_5 + \text{Rh6G (ads.)}$  was 5 mg·g<sup>-1</sup> (see Section 3.1), which means that in a working suspension with a concentration of 0.1 g·L<sup>-1</sup>, the quantity of Rh6G is 10–6 mol per liter. As depicted in Figure 10a, the pristine Rh6G solution exhibits a high PL intensity with a peak at 552 nm. Further investigations focusing on the utilization of pristine Rh6G as a sensor have revealed that there is no linear correlation between the PL intensity and carbamazepine concentration in this system (Figure 10b). Interestingly, the PL intensity shows inconsistent behavior, increasing in some cases while decreasing in others. Furthermore, the peak position remains stable without any noticeable shift. Based on these observations, it can be concluded that pristine Rhodamine 6G is not suitable for use as a sensor in carbamazepine determination.

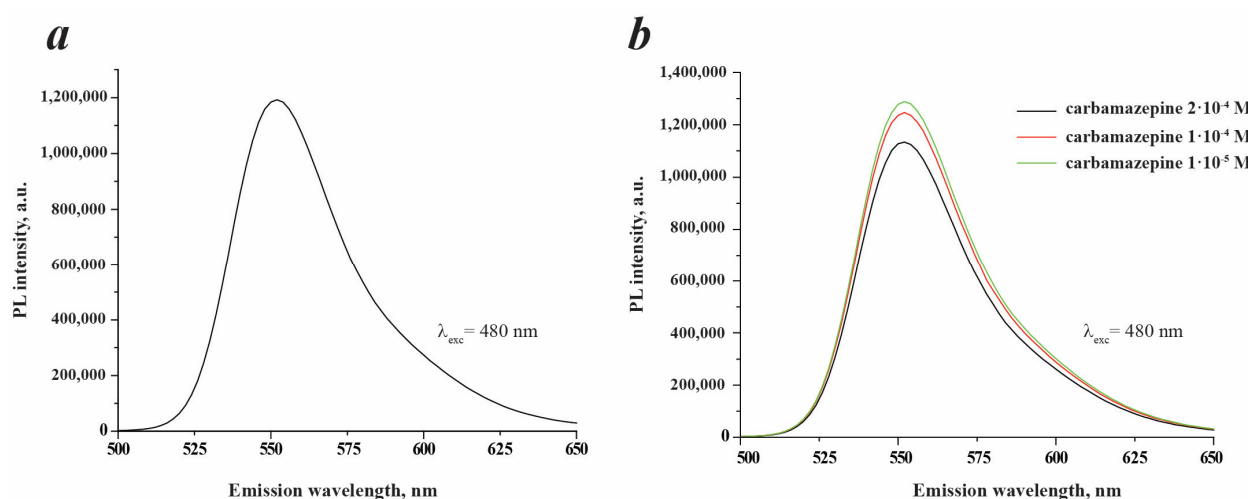


**Figure 10.** PL spectra of blank Rh6G solution with concentration  $10^{-6} \text{ M}$  (**a**) and Rh6G with concentration  $10^{-6} \text{ M}$  in the presence of carbamazepine of different concentrations (**b**). 0.1 M KCl was used as a solvent in all experiments.

It is worth noting that a significant red shift in the peak position of pristine Rhodamine 6G (Rh6G) was observed after anchoring it to silica particles. The peak position shifted from 518 nm to 545 nm, indicating a  $\Delta$  of 27 nm. This observation provides evidence of the formation of hydrogen bonds between the fluorophore molecule and silica particles. These hydrogen bonds restrict the intramolecular rotation mechanism of the fluorophore, leading to improved photoluminescence (PL) properties (see (2) in Figure 2) [29,44]. Furthermore, the lower red shift from 545 nm to 549 nm has been noticed on the PL spectrum of  $\text{SiO}_2/\equiv\text{Si}(\text{CH}_2)_3\text{NH}_2/\equiv\text{SiC}_6\text{H}_5 + \text{Rh6G (ads.)}$  after the addition of carbamazepine (Figure 9c). It is suggested that the amino and C=O groups present in the silica–Rhodamine 6G system, which possesses a lone electron pair, participate in sensing carbamazepine by forming hydrogen bonds with the -C(=O)-NH<sub>2</sub> functionalities of the carbamazepine molecule. This interaction leads to an increase in PL intensities. Additionally,  $\pi$ - $\pi$  interactions between the phenyl and xanthene ring of Rh6G and the carbamazepine conjugated system are also possible. These interactions contribute to intra- and intermolecular charge transfers, enhancing the photoluminescence intensity. However, it is challenging to determine precisely which groups are involved, as it depends on their availability. Nonetheless, the presence of multiple interaction sites is advantageous for the detection of the analyte. The proposed mechanism is schematically illustrated in Figure 11.

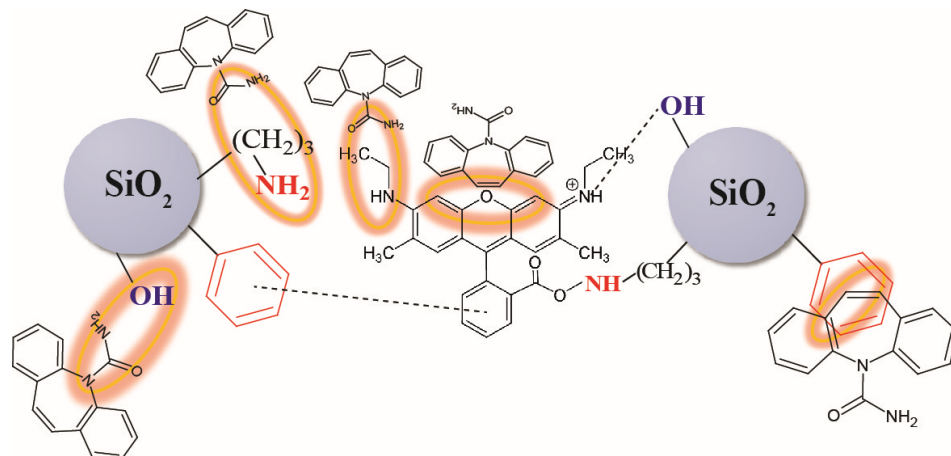


**Figure 11.** Scheme of the proposed sensing mechanism of carbamazepine by synthesized particles.

#### 4. Conclusions

A luminescent system consisting of bifunctional  $\text{SiO}_2/\equiv\text{Si}(\text{CH}_2)_3\text{NH}_2/\equiv\text{SiC}_6\text{H}_5$  particles with anchored Rh6G for the detection of carbamazepine using a ‘turn-on’ approach was developed. It has been shown that the highest photoluminescence is demonstrated by a suspension of a silica sample with physically adsorbed Rhodamine 6G. The best-performing sample consists of spherical particles with a size of approximately 241 nm and a positive charge of 33.3 mV when in an aqueous solution. Elemental analysis, titration, thermogravimetry, and IR data have indicated the presence of a small amount of physically adsorbed dye on the surface of silica particles that bear 3-aminopropyl and phenyl groups. The combination of these groups and the ‘mobile’ fixation of the dye allows the material to exhibit a high photoluminescence response in aqueous suspensions and, therefore, to be applied in drug sensing. Studies have demonstrated that the photoluminescent properties of the suspensions remain unaffected within the ionic strengths range of 0.1 to  $1 \text{ g}\cdot\text{L}^{-1}$ . However, the absence of ions leads to a decrease in photoluminescence. Furthermore, it has been observed that the suspension remains stable for a duration of up to 5 days. This sensor has exhibited a linear response to carbamazepine (neuropathic medicine) within the concentration range of 0.8–200.0  $\mu\text{M}$ . It was determined the limit of detection of the sensor was 17.9  $\mu\text{M}$  (equivalent to  $4.2 \text{ mg}\cdot\text{L}^{-1}$ ), and the limit of quantification was found to be 59.7  $\mu\text{M}$  (equivalent to  $14.1 \text{ mg}\cdot\text{L}^{-1}$ ). It was revealed that ofloxacin did not affect the sensor response towards carbamazepine in simultaneous presence in solution. The presence of other antibiotics slightly influenced the sensor response. To eliminate this effect, the pre-treatment of real water is required. The hypothesis concerning the sensing mechanism has been proposed and consists of the formation of hydrogen bonds between carbamazepine molecules and available oxygen- and nitrogen-containing moieties of  $\text{SiO}_2/\equiv\text{Si}(\text{CH}_2)_3\text{NH}_2/\equiv\text{SiC}_6\text{H}_5 + \text{Rh6G (ads.)}$ .

**Author Contributions:** Conceptualization, I.M. and H.Y.; formal analysis, I.M., E.D., V.K. and H.Y.; resources, M.V. and I.M.; data curation, I.M. and H.Y.; writing—original draft preparation, I.M. and H.Y.; writing—review and editing, H.Y., E.D., M.V., V.K. and I.M.; supervision, I.M.; funding acquisition, I.M. and H.Y. All authors have read and agreed to the published version of the manuscript.

**Funding:** This research was carried out under the APVV-19-0302 project and Štefan Schwarz Postdoc Fellowship No. 2022/OV1/010.

**Institutional Review Board Statement:** Not applicable.

**Informed Consent Statement:** Not applicable.

**Data Availability Statement:** Data will be available upon request.

**Conflicts of Interest:** The authors declare no conflict of interest.

#### References

1. Xue, X.; Jia, J.; Yue, X.; Guan, Y.; Zhu, L.; Wang, Z. River contamination shapes the microbiome and antibiotic resistance in sharpbelly (*Hemiculter leucisculus*). *Environ. Pollut.* **2021**, *268*, 115796. [[CrossRef](#)] [[PubMed](#)]
2. Rajawat, G.S.; Belubbi, T.; Nagarsenker, M.S.; Abrahamsson, B.; Cristofoletti, R.; Groot, D.W.; Langguth, P.; Parr, A.; Polli, J.E.; Mehta, M.; et al. Biowaiver monograph for immediate-release solid oral dosage forms: Carbamazepine. *J. Pharm. Sci.* **2021**, *110*, 1935–1947.
3. Miao, X.-S.; Metcalfe, C.D. Determination of carbamazepine and its metabolites in aqueous samples using liquid chromatography–electrospray tandem mass spectrometry. *Anal. Chem.* **2003**, *75*, 3731–3738. [[CrossRef](#)]
4. Shankar Kikkeri, N.; Nagalli, S. Trigeminal Neuralgia. In *StatPearls*; StatPearls Publishing: Treasure Island, FL, USA, 2022.
5. Köhling, R. Voltage-gated sodium channels in epilepsy. *Epilepsia* **2002**, *43*, 1278–1295. [[CrossRef](#)] [[PubMed](#)]
6. Speed, D.; Dickson, S.; Cairns, E.; Kim, N. Analysis of six anticonvulsant drugs using solid-phase extraction, deuterated internal standards, and gas chromatography-mass spectrometry. *J. Anal. Toxicol.* **2000**, *24*, 685–690. [[CrossRef](#)] [[PubMed](#)]
7. Weigel, S.; Bester, K.; Hühnerfuss, H. New method for rapid solid-phase extraction of large-volume water samples and its application to non-target screening of North Sea water for organic contaminants by gas chromatography-mass spectrometry. *J. Chromatogr. A* **2001**, *912*, 151–161. [[CrossRef](#)]
8. Öllers, S.; Singer, H.P.; Fässler, P.; Müller, S.R. Simultaneous quantification of neutral and acidic pharmaceuticals and pesticides at the low- $\text{ng}/\text{l}$  level in surface and waste water. *J. Chromatogr. A* **2001**, *911*, 225–234. [[CrossRef](#)]

9. Mansour, N.M.; El-Sherbiny, D.T.; Ibrahim, F.A.; El Subbagh, H.I. Development of an Inexpensive, sensitive and green HPLC method for the simultaneous determination of brivaracetam, piracetam and carbamazepine; application to pharmaceuticals and human plasma. *Microchem. J.* **2021**, *163*, 105863. [[CrossRef](#)]
10. Miao, X.-S.; Yang, J.-J.; Metcalfe, C.D. Carbamazepine and its metabolites in wastewater and in biosolids in a municipal wastewater treatment plant. *Environ. Sci. Technol.* **2005**, *39*, 7469–7475. [[CrossRef](#)]
11. Zhou, S.; Xu, L.; Liu, L.; Kuang, H.; Xu, C. Development of a monoclonal antibody-based immunochromatographic assay for the detection of carbamazepine and carbamazepine-10, 11-epoxide. *J. Chromatogr. B* **2020**, *1141*, 122036. [[CrossRef](#)]
12. Qambrani, N.; Buledi, J.A.; Khand, N.H.; Solangi, A.R.; Ameen, S.; Jalbani, N.S.; Khatoon, A.; Taher, M.A.; Moghadam, A.T.; Shojaei, M.; et al. Facile synthesis of NiO/ZnO nanocomposite as an effective platform for electrochemical determination of carbamazepine. *Chemosphere* **2022**, *303*, 135270. [[CrossRef](#)] [[PubMed](#)]
13. Ramos, I.I.; Carl, P.; Schneider, R.J.; Segundo, M.A. Automated lab-on-valve sequential injection ELISA for determination of carbamazepine. *Anal. Chim. Acta* **2019**, *1076*, 91–99. [[CrossRef](#)] [[PubMed](#)]
14. Khayoon, W.S.; Younis, H.R. Ion pair-dispersive liquid–liquid microextraction combined with spectrophotometry for carbamazepine determination in pharmaceutical formulations and biological samples. *J. Anal. Chem.* **2020**, *75*, 733–741. [[CrossRef](#)]
15. Rezaei, Z.; Hemmateenejad, B.; Khabnadideh, S.; Gorgin, M. Simultaneous spectrophotometric determination of carbamazepine and phenytoin in serum by PLS regression and comparison with HPLC. *Talanta* **2005**, *65*, 21–28. [[CrossRef](#)] [[PubMed](#)]
16. Goudarzy, F.; Zolgharnein, J.; Ghasemi, J.B. Determination and degradation of carbamazepine using g-C<sub>3</sub>N<sub>4</sub>@CuS nanocomposite as a sensitive fluorescence sensor and efficient photocatalyst. *Inorg. Chem. Commun.* **2022**, *141*, 109512. [[CrossRef](#)]
17. Li, Y.; Sun, M.; Yang, Y.; Meng, H.; Wang, Q.; Li, C.; Li, G. Luminescence-colour-changing sensing toward neurological drug carbamazepine in water and biofluids based on white light-emitting CD/Ln-MOF/PVA test papers. *J. Mater. Chem. C* **2021**, *9*, 8683–8693. [[CrossRef](#)]
18. Halicka, K.; Meloni, F.; Czok, M.; Spychalska, K.; Baluta, S.; Malecha, K.; Pilo, M.I.; Cabaj, J. New Trends in Fluorescent Nanomaterials-Based Bio/Chemical Sensors for Neurohormones Detection- A Review. *ACS Omega* **2022**, *7*, 33749–33768. [[CrossRef](#)]
19. Ziarani, G.M.; Khademi, M.; Mohajer, F.; Badiei, A. The application of modified SBA-15 as a chemosensor. *Curr. Nanomater.* **2022**, *7*, 4–24. [[CrossRef](#)]
20. Willner, M.R.; Vikesland, P.J. Nanomaterial enabled sensors for environmental contaminants. *J. Nanobiotechnol.* **2018**, *16*, 1–16. [[CrossRef](#)]
21. Würth, C.; González, M.G.; Niessner, R.; Panne, U.; Haisch, C.; Genger, U.R. Determination of the absolute fluorescence quantum yield of rhodamine 6G with optical and photoacoustic methods—Providing the basis for fluorescence quantum yield standards. *Talanta* **2012**, *90*, 30–37. [[CrossRef](#)]
22. Ma, C.; Lin, L.; Du, Y.; Chen, L.B.; Luo, F.; Chen, X. Fluorescence quenching determination of iron (III) using rhodamine 6G hydrazide derivative. *Anal. Methods* **2013**, *5*, 1843–1847. [[CrossRef](#)]
23. Xu, Z.Q.; Mao, X.J.; Wang, Y.; Wu, W.N.; Mao, P.D.; Zhao, X.L.; Li, H.J. Rhodamine 6G hydrazone with coumarin unit: A novel single-molecule multianalyte (Cu<sup>2+</sup> and Hg<sup>2+</sup>) sensor at different pH value. *RSC Adv.* **2017**, *7*, 42312–42319. [[CrossRef](#)]
24. Upadhyay, Y.; Paira, P.; Kumar, S.A.; Choi, H.J.; Kumar, R.; Sahoo, S.K. Vitamin B6 cofactor conjugated rhodamine 6G derivative: Fluorescent turn-on sensing of Al (III) and Cr (III) with bioimaging application in live HeLa cells. *Inorg. Chim. Acta* **2019**, *489*, 198–203. [[CrossRef](#)]
25. Zhang, F.; Zhu, J.; Li, J.J.; Zhao, J.W. Fluorescence spectral detection of cysteine based on the different medium-coated gold nanorods-Rhodamine 6G probe: From quenching to enhancement. *Sens. Actuators B Chem.* **2015**, *220*, 1279–1287. [[CrossRef](#)]
26. Yan, G.; Kong, B.; Zhao, J.; Ni, H.; Zhan, L.; Huang, C.; Zou, H. Fluorescence turn-on Cu<sup>2+</sup>-xSe@ HA-rhodamine 6G FRET nanoprobe for hyaluronidase detection and imaging. *J. Photochem. Photobiol. B: Biol.* **2022**, *233*, 112496. [[CrossRef](#)]
27. Kotsyuda, S.S.; Tomina, V.V.; Zub, Y.L.; Furtat, I.M.; Lebed, A.P.; Vaclavikova, M.; Melnyk, I.V. Bifunctional silica nanospheres with 3-aminopropyl and phenyl groups. Synthesis approach and prospects of their applications. *Appl. Surf. Sci.* **2017**, *420*, 782–791. [[CrossRef](#)]
28. Arbeloa, F.L.; Ojeda, P.R.; Arbeloa, I.L. Dimerization and trimerization of rhodamine 6G in aqueous solution. Effect on the fluorescence quantum yield. *J. Chem. Soc. Faraday Trans. 2 Mol. Chem. Phys.* **1988**, *84*, 1903–1912. [[CrossRef](#)]
29. Chen, Z.; Tang, Y.J.; Xie, T.T.; Chen, Y.; Li, Y.Q. Fluorescence spectral properties of rhodamine 6G at the silica/water interface. *J. Fluoresc.* **2008**, *18*, 93–100. [[CrossRef](#)]
30. Shrivastava, A.; Gupta, V.B. Methods for the determination of limit of detection and limit of quantitation of the analytical methods. *Chron. Young Sci.* **2011**, *2*, 21–25. [[CrossRef](#)]
31. Ndlovu, T.; Chimonyo, M.; Okoh, A.I.; Muchenje, V.; Dzama, K.; Raats, J.G. Assessing the nutritional status of beef cattle: Current practices and future prospects. *Afr. J. Biotechnol.* **2007**, *6*, 2727–2734.
32. Harrington, J.M.; Young, D.J.; Essader, A.S.; Sumner, S.J.; Levine, K.E. Analysis of human serum and whole blood for mineral content by ICP-MS and ICP-OES: Development of a mineralomics method. *Biol. Trace Elem. Res.* **2014**, *160*, 132–142. [[CrossRef](#)] [[PubMed](#)]
33. Melnyk, I.V.; Tomina, V.V.; Stolyarchuk, N.V.; Seisenbaeva, G.A.; Kessler, V.G. Organic dyes (acid red, fluorescein, methylene blue) and copper(II) adsorption on amino silica spherical particles with tailored surface hydrophobicity and porosity. *J. Mol. Liq.* **2021**, *336*, 116301. [[CrossRef](#)]

34. Gheitarani, B.; Golshan, M.; Hosseini, M.S.; Salami-Kalajahi, M. Reflectance and photophysical properties of rhodamine 6G/2-(4-methyl-2-oxo-2H-chromen-7-yloxy) acetic acid as a cold hybrid colorant. *Sci. Rep.* **2022**, *12*, 6145. [[CrossRef](#)] [[PubMed](#)]
35. Sing, K.S.W.; Everett, D.; Haul, R.; Moscou, L.; Pierotti, R.; Rouquerol, J.; Siemieniewska, T. International union of pure commission on colloid and surface chemistry including catalysis\* reporting physisorption data for gas/solid systems with special reference to the determination of surface area and porosity. *Pure Appl. Chem.* **1985**, *57*, 603–619. [[CrossRef](#)]
36. Majoube, M.; Henry, M. Fourier transform Raman and infrared and surface-enhanced Raman spectra for rhodamine 6G. *Spectrochim. Acta Part A Mol. Spectrosc.* **1991**, *47*, 1459–1466. [[CrossRef](#)]
37. Halford, J.J. One Ring to Dissolve Them All: One Ring to Dissolve Them All. *Epilepsy Curr.* **2015**, *15*, 52–53. [[CrossRef](#)]
38. Ferdig, M.; Kaleta, A.; Buchberger, W. Improved liquid chromatographic determination of nine currently used (fluoro) quinolones with fluorescence and mass spectrometric detection for environmental samples. *J. Sep. Sci.* **2005**, *28*, 1448–1456. [[CrossRef](#)]
39. Jara, B.; Tucca, F.; Srain, B.M.; Mejanelle, L.; Aranda, M.; Fernández, C.; Pantoja-Gutiérrez, S. Antibiotics florfenicol and flumequine in the water column and sediments of Puyuhuapi Fjord, Chilean Patagonia. *Chemosphere* **2021**, *275*, 130029. [[CrossRef](#)]
40. Tamtam, F.; Mercier, F.; Le Bot, B.; Eurin, J.; Tuc Dinh, Q.; Clement, M.; Chevreuil, M. Occurrence and fate of antibiotics in the Seine River in various hydrological conditions. *Sci. Total Environ.* **2008**, *393*, 84–95. [[CrossRef](#)]
41. Zounková, R.; Klimešová, Z.; Nepejchalová, L.; Hilscherová, K.; Bláha, L. Complex evaluation of ecotoxicity and genotoxicity of antimicrobials oxytetracycline and flumequine used in aquaculture. *Environ. Toxicol. Chem.* **2011**, *30*, 1184–1189. [[CrossRef](#)]
42. Lee, H.B.; Peart, T.E.; Svoboda, M.L. Determination of ofloxacin, norfloxacin, and ciprofloxacin in sewage by selective solid-phase extraction, liquid chromatography with fluorescence detection, and liquid chromatography–tandem mass spectrometry. *J. Chromatogr. A* **2007**, *1139*, 45–52. [[CrossRef](#)] [[PubMed](#)]
43. Turiel, E.; Bordin, G.; Rodríguez, A.R. Trace enrichment of (fluoro) quinolone antibiotics in surface waters by solid-phase extraction and their determination by liquid chromatography–ultraviolet detection. *J. Chromatogr. A* **2003**, *1008*, 145–155. [[CrossRef](#)] [[PubMed](#)]
44. Cha, I.; Baek, S.; Song, S.G.; Kim, J.; Lee, H.K.; Lee, J.; Song, C. Inter-and Intra-Hydrogen Bonding Strategy to Control the Fluorescence of Acylhydrazone-Based Conjugated Microporous Polymers and Their Application to Nitroaromatics Detection. *Macromol* **2021**, *1*, 234–242. [[CrossRef](#)]

**Disclaimer/Publisher's Note:** The statements, opinions and data contained in all publications are solely those of the individual author(s) and contributor(s) and not of MDPI and/or the editor(s). MDPI and/or the editor(s) disclaim responsibility for any injury to people or property resulting from any ideas, methods, instructions or products referred to in the content.